Journal of Power Sources 299 (2015) 49–56

Contents lists available at ScienceDirect

Journal of Power Sources

journal homepage: www.elsevier.com/locate/jpowsour

Incorporation of conductive polymer into soft carbon electrodes for lithium ion capacitors

Young-Geun Lim [a, b], Min-Sik Park [a, **], Ki Jae Kim [a, *], Kyu-Sung Jung [c], Jung Ho Kim [d], Mohammed Shahabuddin [e], Dongjin Byun [b, ***], Ji-Sang Yu [a]

[a] Advanced Batteries Research Center, Korea Electronics Technology Institute, Seongnam, Gyeonggi 463-816, Republic of Korea
[b] Department of Materials Science and Engineering, Korea University, Seoul 136-701, Republic of Korea
[c] Mobile Battery Division, LG-Chem, Daejeon, 305-738, Republic of Korea
[d] Institute for Superconducting and Electronic Materials (ISEM), University of Wollongong, North Wollongong, NSW 2500, Australia
[e] Department of Physics and Astronomy, College of Science, King Saud University, P.O. Box 2455, Riyadh 11451, Saudi Arabia

HIGHLIGHTS

- Incorporation of conductive PEDOT-PSS allows a faster Li^+ insertion into soft carbon.
- The soft carbon with 1.0 wt% PEDOT-PSS exhibits a capacity retention of 64% at 5 C.
- The LIC with 1.0 wt% PEDOT-PSS retains 85% of initial capacitance after 5000 cycles.

GRAPHICAL ABSTRACT

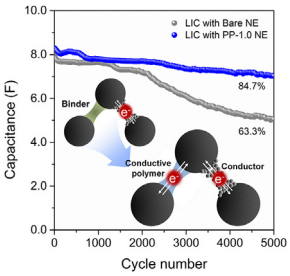

ARTICLE INFO

Article history:
Received 22 June 2015
Received in revised form
29 July 2015
Accepted 23 August 2015
Available online xxx

Keywords:
Lithium ion capacitor
Negative electrode
Soft carbon
Conductive polymer

ABSTRACT

The positive effects of incorporating electrically conductive poly(3,4-ethylenedioxythiophene)-polystyrene sulfonate (PEDOT-PSS) into the negative electrode (NE) of a lithium ion capacitor (LIC) is investigated. The binding material of the NE, styrene-butadiene rubber (SBR), is partially substituted by conductive PEDOT-PSS. The soft carbon NE with 1.0 wt% PEDOT-PSS exhibits enhanced capacity retention of 64% at a current density of 5 C by lowering its electrical and electrochemical charge transfer resistance. The rate capability increased with increasing amounts of PEDOT-PSS, with no variation in the Li^+ diffusivity. This improved electrochemical performance of the NE is also reflected in the LIC full-cell configuration. An LIC employing a 1.0 wt% PEDOT-PSS NE delivers 6.6 F at a high current density of 100 C, which is higher than the 6.0 F measured for the LIC with a bare NE. Moreover, the LIC with the 1.0 wt% PEDOT-PSS NE retains 85% of its initial capacitance even after 5000 cycles. These results are mainly attributed to the favourable electrical network formed by the incorporation of PEDOT-PSS into the NE. Thus, we believe that the incorporation of conductive PEDOT-PSS is a viable approach for obtaining high-power LICs.

1. Introduction

Electrochemical double-layer capacitors (EDLCs) are the most promising energy storage devices for power quality applications in

* Corresponding author. Tel.: +82 31 789 7492; fax: +82 31 789 7499.
** Corresponding author. Tel.: +82 31 789 7496; fax: +82 31 789 7499.
*** Corresponding author. Tel.: +82 2 3290 3280; fax: +82 2 928 3584.
E-mail addresses: parkms@keti.re.kr (M.-S. Park), kijaekim@keti.re.kr (K.J. Kim), dbyun@korea.ac.kr (D. Byun).

http://dx.doi.org/10.1016/j.jpowsour.2015.08.083
0378-7753/

portable electronics, electric transportation, and renewable energy generation [1–4]. Although EDLCs that offer high power capability and excellent cycle life have already been commercialized, their energy density is still limited as compared with rechargeable batteries [5–7]. There is therefore keen interest in further increasing the energy density of EDLCs for extending their application to transportation or stationary energy storage. A number of hybrid capacitors have been proposed with this goal in mind, with asymmetric cell configurations that allow for improved energy density [8–11]. Lithium ion capacitors (LICs), known as promising hybrid capacitors, have also attracted much attention because they can provide approximately three times higher energy density than conventional EDLCs [8,12–16].

LICs are composed of activated carbon as a positive electrode (PE) and Li^+-inserting materials (*e.g.* graphite, hard carbon, soft carbon, and $Li_4Ti_5O_{12}$) as a negative electrode (NE). In contrast to the symmetric electrochemical behaviour of EDLCs, LICs show asymmetric charge–discharge profiles that combine a non-Faradaic reaction (adsorption/desorption of anions) in the PE and a Faradaic reaction (insertion/extraction of Li^+) in the NE close to 0 V *vs.* Li/Li^+. This enables a higher operating voltage up to ~4.2 V, which is much higher than that of conventional EDLCs (~3.0 V). In this hybrid configuration, however, the power capability and cycle performance of LICs are strongly dependent on the material characteristics of the NE because the Li^+ insertion/extraction in the NE is much slower than its counter reaction in the PE. Among the various NE materials, graphite is considered a promising candidate as it allows the most extended operating voltage of LICs owing to its low and flat redox potential of approximately 0 V *vs.* Li/Li^+. However, graphite suffers from its poor rate capability and cycle performance arising from the sluggish kinetics of Li^+ mobility in the highly ordered crystal structure. In contrast, as proposed by Amatucci et al. [8] $Li_4Ti_5O_{12}$ shows great promise as a suitable NE material for LICs because of its excellent rate capability and cycle performance [17–19], but the high redox potential of $Li_4Ti_5O_{12}$ of approximately 1.5 V *vs.* Li/Li^+ limits the practical operating voltage of LICs (1.0–3.2 V).

On the other hand, soft carbon is a suitable choice for ensuring not only good rate capability and cycle performance but also a relatively extended operating voltage for LICs. In practice, soft carbon has numerous intercalation channels of Li^+, good structural stability, and a low reaction voltage profile owing to its low crystallinity, characteristics that are mainly responsible for the good rate capability and cycle performance [20,21]. Despite such advantages, it is crucial to enhance the Li^+ insertion and extraction characteristics of soft carbon for further improvement of current LICs. One possible approach is to incorporate electrical conductive polymers such as polyaniline, polyacetylene, polypyrrole, and polythiophene into the NE. As confirmed by many studies, conductive polymers can effectively improve the electrode performance of batteries or capacitors [22–25] by utilizing additional electric conduction pathways and minimizing charge transfer resistance during cycling.

Herein, we propose incorporating poly(3,4-ethylenedioxythiophene)-polystyrene sulfonate (PEDOT-PSS) into a soft carbon electrode as the NE, and we demonstrate the improved electrochemical performance of the NE for practical use in LICs. The incorporation of PEDOT-PSS enhances the electrical conductivity of the NE and, by extension, the electrochemical performance of the LIC because it is highly conductive, mechanically durable, stable in the oxidized state, and insoluble in common carbonate solvents (*e.g.* electrolytes). Accordingly, partial substitution of a conventional polymer binder with the conductive PEDOT-PSS in the NE allows the formation of an additional electrical network between the active material particles. It is essential for improving the rate capability of the NE without cyclic performance fading. The results show that in comparison with a bare soft carbon NE, incorporating PEDOT-PSS improves the electrochemical performances of LICs.

2. Experimental

2.1. Preparation of electrodes

The bare NE was prepared with a slurry containing 90 wt% soft carbon (GS Energy Co., Korea), 5 wt% conducting carbon (Super-P, TIMCAL Co.), 2.5 wt% carboxymethyl cellulose (CMC), and 2.5 wt% styrene-butadiene rubber (SBR) in distilled water. Meanwhile, the SBR was partially substituted with 0.5 wt% and 1.0 wt% PEDOT-PSS (Sigma–Aldrich Co.) for preparation of the NEs, which were denoted as PP-0.5 NE and PP-1.0 NE, respectively. The slurries were applied to a mesh-type Cu current collector using vertical coating equipment and the loading amount was fixed at 6.5 mg cm^{-2} for each NE. The NEs were dried in a convection oven and roll-pressed up to density of 0.6 g cm^{-3}. The PE was prepared following the same procedure as the NEs using Al mesh with 80 wt% activated carbon (MSP-20, Kansai Coke and Chemicals Co.), 10 wt% conducting carbon (Super-P), and 10 wt% PVdF (polyvinylidene fluoride, Sigma–Aldrich Co.). The PE had a loading amount of 5.2 mg cm^{-2} and a density of 0.5 g cm^{-3}. The detailed specifications of the soft carbon NEs are provided in Table S2. The PEDOT-PSS incorporation into the NEs was confirmed by Fourier transform infrared spectroscopy (FT-IR, PerkinElmer Co.) and X-ray photoelectron spectroscopy (XPS, Thermo Scientific Co.). The electrical conductivity of the as-prepared NEs was measured by the four-point probe method.

2.2. Electrochemical measurements

Half-cell test – CR2032 coin-type half-cells were assembled in a dry room by stacking a working electrode, a separator (polyethylene, Asahi Co.), and a metallic Li counter electrode. These components were immersed together in an electrolyte consisting of 1.3 M $LiPF_6$ in ethylene carbonate/dimethyl carbonate (EC/DMC, 3:7 volume ratio, PANAX E-tec Co.). The rate capability was examined in the voltage range of 0.01–1.5 V (*vs.* Li/Li^+) at current densities from 0.2 C (50 mA g^{-1}) to 5 C (1250 mA g^{-1}) using a battery tester (MACCOR series 4000). For the electrochemical impedance spectroscopy (EIS) measurements, a metallic Li reference electrode was added to the above mentioned half-cell configuration and the cells were evaluated within the frequency range of 1.0 MHz–10 mHz.

Full-cell test – Pouch-type LIC full cells 34 × 50 mm in size were assembled in a dry room using the same electrolyte and separator as for the half cell. Li^+ pre-doping into the NE, an essential lithiation process for proper operation of LICs, was carried out using an auxiliary Li metal electrode under a constant voltage of 0.01 V (*vs.* Li/Li^+) and the doping level was carefully controlled to be 80% of the practical capacity of the soft carbon NE (250 mAh g^{-1}). The LICs were galvanostatically charged and discharged at current densities from 0.2 C (17 mA g^{-1}) to 200 C (17 A g^{-1}) in the voltage range of 1.5–3.9 V. The cycling performance was tested with a constant current of 10 C (850 mA g^{-1}) over 5000 cycles, and EIS was performed under the same conditions as for the half-cell.

3. Results and discussion

The PP-0.5 and PP-1.0 NEs were prepared by partial substitution of SBR binder with 0.5 and 1.0 wt% of conductive PEDOT-PSS polymer, respectively, to investigate the effects of PEDOT-PSS incorporation on the electrochemical performance of soft carbon NEs. Unlike the insulating SBR binder, it is expected that PEDOT-PSS

can improve the electrochemical performance of soft carbon NEs by reducing the electrical and electrochemical charge transfer resistance, particularly during Li^+ insertion, owing to its high electric conductivity of 2.22 S cm^{-1}. First of all, the morphological change of the NEs after PEDOT-PSS incorporation was investigated by using a field-emission scanning electron microscope (FESEM). As seen in the FESEM image of the bare NE (Fig. 1a), soft carbon particles approximately 9–11 μm in size were uniformly coated onto Cu mesh with a thickness of 108 μm, as evidenced by the cross-sectional FESEM image (Fig. 1b). After 1.0 wt% of PEDOT-PSS incorporation, the NE showed a similar morphology and microstructure, as shown in Fig. 1c and d, respectively. Thus, we confirmed that the partial incorporation of PEDOT-PSS does not induce any morphological change of the NE.

For further structural inspection, we conducted Fourier transform infrared spectroscopy (FT-IR) and X-ray photoelectron spectroscopy (XPS) analyses for the as-prepared NEs and the results are given in Fig. 2. The incorporation of PEDOT-PSS is evident in the FT-IR spectra (Fig. 2a). All three NEs show a peak arising from aromatic C=C bonds at 1650 cm^{-1}, which is associated with the turbostratic carbon of the graphene layer. The S=O (1350 cm^{-1}), S=O (1150–1350 cm^{-1}), and S–O–R (800–900 cm^{-1}) peaks are observed for both the PP-0.5 and the PP-1.0 NEs but not for the bare NE. These noticeable S signals are mainly attributed to the incorporated PEDOT-PSS, and their intensities increase with increasing PEDOT-PSS concentration. These results are further confirmed by the XPS analysis, as shown in Fig. 2b. There is no evidence for S in the S 2p spectrum obtained from the bare NE, whereas two distinct peaks of PEDOT-PSS are observed for both the PP-0.5 and the PP-1.0 NEs. The peak at the lower binding energy, corresponding to the PEDOT component, is de-convoluted into spin-split species at 164.5 eV (*2p 3/2*) and 165.6 eV (*2p 1/2*), with a binding energy difference of 1.1 eV [26]. Another peak detected at a higher binding energy of approximately 169.0 eV, originating from the S atoms in PSS, has two components, one at 168.7 and 169.9 eV, which are associated with PSS^--Na^+ groups, and the other at 170.8 eV, which is attributed to PSSH [26,27]. The PEDOT-PSS is thereby well-incorporated in the NEs and would improve the electrical conductivity of the NEs. As expected, the PP-1.0 NE has a higher electric conductivity (2.22 S cm^{-1}) than the PP-0.5 (1.98 S cm^{-1}) and bare NEs (1.74 S cm^{-1}), as summarized in Table 1. This is because the well-dispersed PEDOT-PSS provides additional electron conduction pathways between soft carbon particles and, by extension, at the interface between the active material and the current collector in the NEs. Moreover, this increased electric conductivity could facilitate Li^+ mobility by reducing electrical contact resistance in the NEs. As supposed, the electrical enhancement is more evident when the amount of PEDOT-PSS increases. However, the incorporation of PEDOT-PSS would not significantly affect the wettability of the NEs (Fig. 2c). In addition, substitution of SBR binder of more than 1.0 wt% would lead to the degradation of adhesion between the active material and the current collector (Fig. S2).

The effects of PEDOT-PSS incorporation on the electrochemical performance of the soft carbon NE were examined. Fig. 3a shows galvanostatic voltage profiles recorded at a constant current density of 0.2 C (50 mA g^{-1}) in the first cycle. All the NEs delivered similar charge (Li^+ insertion) and discharge (Li^+ extraction) capacities of approximately 290.2 mAh g^{-1} and 250.1 mAh g^{-1}, respectively. The relatively low initial coulombic efficiency of ~86.2% is mainly attributed to the irreversible charge consumption of the soft carbon NE by forming solid electrolyte interphase (SEI) films on the surface [28–30]. After the first cycle, all NEs exhibited a high coulombic efficiency of 98.5% during subsequent cycles (Table S3). Thus, it should be noted that the PEDOT-PSS incorporation does not induce any additional irreversible charge consumption during cycling. In addition, the rate capabilities of the NEs

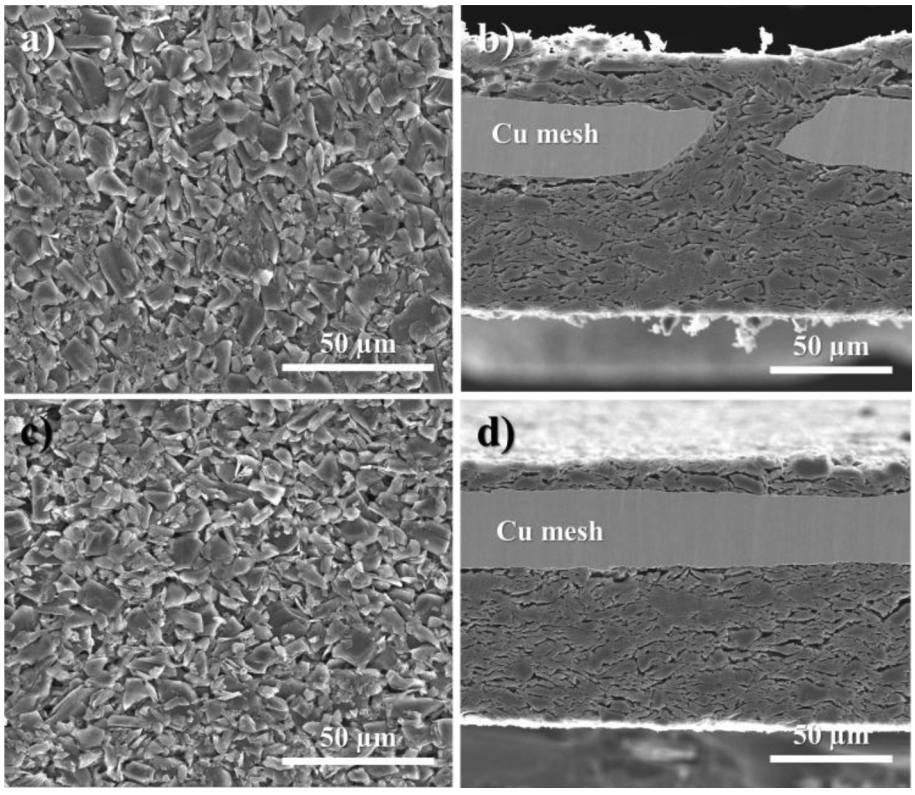

Fig. 1. Surface and cross-sectional FESEM images of (a)–(b) the bare and (c)–(d) the PP-1.0 NEs.

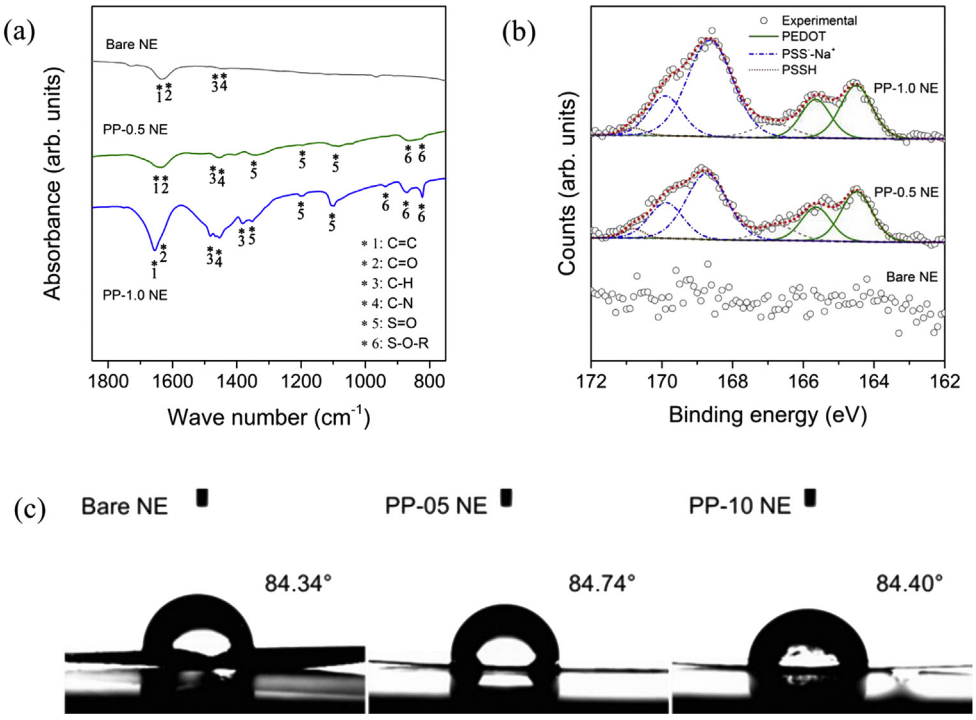

Fig. 2. Comparison of (a) FT-IR spectra, (b) XPS S 2p spectra, and (c) contact angles collected from the bare, PP-0.5, and PP-1.0 NEs.

Table 1
Surface conductivity of the bare, PP-0.5, and PP-1.0 NEs.

Sample	Bare NE	PP-0.5 NE	PP-1.0 NE
Surface conductivity (S cm^{-1})	1.74 (±0.01)	1.98 (±0.01)	2.22 (±0.01)

were also examined (Fig. 3b) at current densities of 0.2 C (50 mA g^{-1}, dash lines) and 5 C (1250 mA g^{-1}, solid lines). At a low current density of 0.2 C, all NEs showed similar charge and discharge capacities of approximately 253.8 mAh g^{-1} and 250.0 mAh g^{-1}, respectively, indicating that the incorporated PEDOT-PSS does not affect the Li^+ storage capability of the NEs.

The effect of PEDOT-PSS incorporation on the electrochemical performance of the NEs was more evident at a high current density of 5 C (1250 mA g^{-1}). The capacity retentions of the PP-0.5 and PP-1.0 NEs were estimated to be 59.0% and 63.8%, respectively, during charge (Li^+ insertion) at a current density of 5 C (Fig. S3), which is much higher than that of the bare NE (30.1%). In particular, the PP-1.0 NE exhibited a high charge capacity of 162 mAh g^{-1} with a coulombic efficiency of 99.9%. The positive effect also reflected in the electrochemical performance of the NEs during discharge (Li^+ extraction). Note that the Li^+ storage capability of soft carbon NE can be more effectively enhanced by PEDOT-PSS incorporation at a high current density (5 C), whereas the effect is negligible at a low current density (0.2 C). This can be reasonably explained by a high overpotential of soft carbon induced by fast Li^+ insertion and extraction at a high current density. The overpotential of the PP-1.0 NE at a current density of 5 C was estimated to be approximately 70 mV, which is comparable to that attained at 0.2 C. In contrast, the bare NE showed a much higher overpotential (430 mV) at 5 C, leading to the significant degradation of Li^+ storage capability (Fig. S4). These results reveal that the PEDOT-PSS incorporation is kinetically effective for the improvement of Li^+ insertion rather than Li^+ extraction. For further comparison of the rate capability, the cells were charged at various current densities and discharged at a fixed current density of 0.2 C and the results are given in Fig. 3c. The PP-0.5 and PP-1.0 NEs exhibited much higher capacity retention than the bare NE above 1 C (250 mA g^{-1}). The bare NE retained only 8.2% of its capacity at 10 C, which is a significantly less than the 34.0% of the PP-0.5 NE and 44.9% of the PP-1.0 NE. For comparison, the cells were charged at a fixed current density of 0.2 C and discharged at various current densities (Fig. 3d). All NEs showed similar capacity retentions of approximately 94%, even at a high current density of 10 C (2500 mA g^{-1}) without significant degradation (Fig. S5). These results also support our claim that the PEDOT-PSS incorporation is more effective for enhancing the kinetics for Li^+ insertion rather than for Li^+ extraction.

To get more details, Nyquist plots of the NEs were obtained at a fully charged state, as shown Fig. 4a. The spectra exhibit depressed arcs at high frequencies and a straight line inclined at a constant angle to the real axis at low frequencies. The results were carefully fitted with an equivalent circuit (inset), which comprises the uncompensated solution resistance (R_s), the surface film resistance (R_f), the constant phase element (CPE_f) for surface films, the charge transfer resistance (R_{ct}), the constant phase element (CPE_{dl}) for double-layer charging/discharging, and the diffusion impedance (Z_d). Note that R_{ct} decreases with increasing amount of PEDOT-PSS incorporation, with 35.5, 30.9, and 26.8 Ω measured for the bare, PP-0.5, and PP-1.0 NEs, respectively (Table 2), indicating that the PEDOT-PSS incorporation is also beneficial for improving Li^+ transport kinetics, as evidenced by the smaller values of R_{ct}. The reduction of R_{ct} of the NEs induced by PEDOT-PSS incorporation was also evident at OCV (Fig. S6 and Table S4). Moreover, there is no significant difference in the Li^+ diffusion coefficient (D_{Li}) among these NEs derived from the Warburg impedance, Z_{Im}, in the diffusion-controlled region as a function of $\omega^{-1/2}$ for the bare, PP-0.5, and PP-1.0 NEs (Fig. 4b). The relationships are linear, and equal Warburg pre-factors (σ) are obtained for all the NEs ($\sigma \approx 3.90$), expressed as follows [31,32].

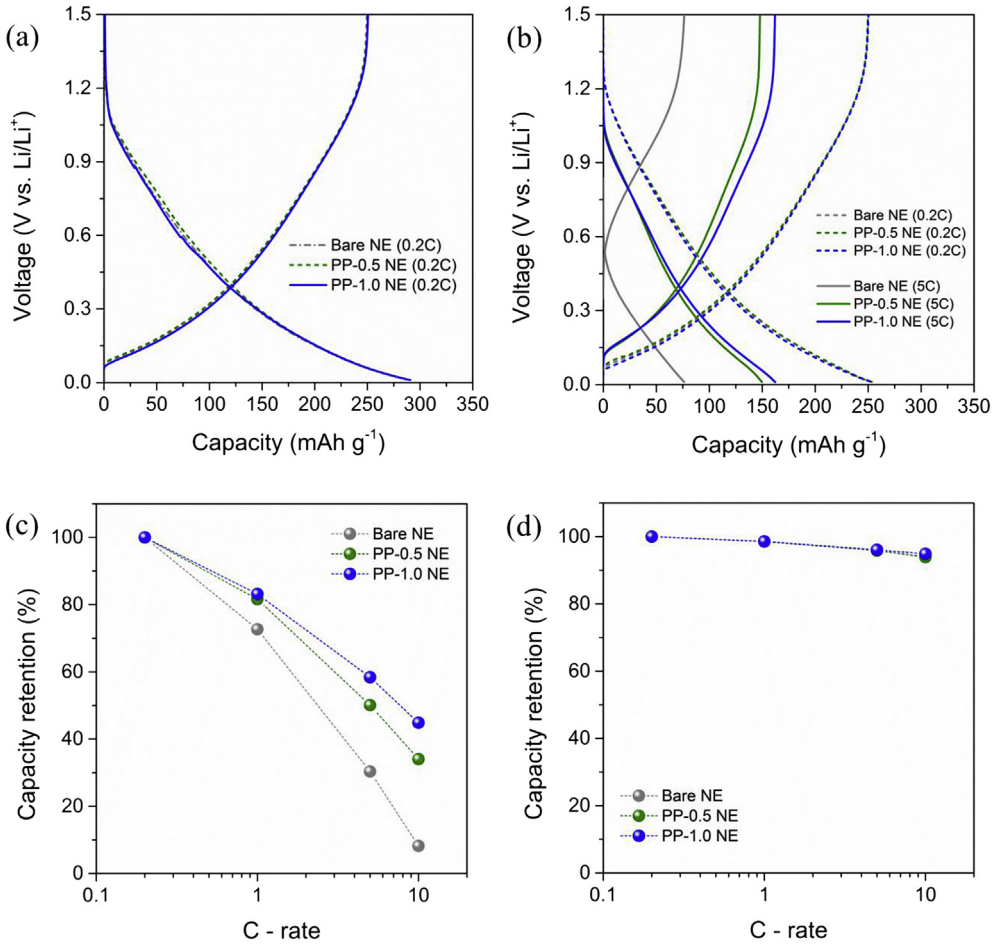

Fig. 3. Electrochemical performance of the NEs in half cell configuration: (a) galvanostatic voltage profiles in the first cycle at a constant current density of 0.2 C, (b) rate capabilities at current densities of 0.2 C and 5 C, (c) capacity retentions at various current densities during charge (the current density was fixed at 0.2 C during discharge), and (d) capacity retentions at various current densities during discharge (the current density was fixed at 0.2 C during charge).

$$\sigma = V_m(dV_{OC}/dx)/zFA(2D_{Li})^{1/2} \quad (1)$$

where V_m was calculated to be 26.12 $cm^3\ mol^{-1}$ based on the mass (4.985 mg) and the volume (10.85×10^{-3} cm^3) of soft carbon. At 100% SOC (assuming that $x = 1.0$ in practical capacity of 250 mAh g^{-1}), the value of dV_{OC}/dx was determined to be 1.146. The surface area (A) of 1.69 $m^2\ g^{-1}$ was obtained from a Brunauer–Emmett–Teller (BET) measurement and the slope of Z_{Im} *vs.* $\omega^{-1/2}$ was measured to be 3.90. As expected from Eq. (1), these parameters are equivalent for all the NEs employing the same soft carbon. Although the diffusion coefficient (D_{Li}) of soft carbon cannot be derived accurately owing to its disordered microstructure, we calculated Eq. (1) by employing the practical capacity (250 mAh g^{-1}) instead of unknown theoretical capacity, and the same D_{Li}, ~4.46×10^{-13} $cm^2\ s^{-1}$, was obtained for all NEs accordingly. Therefore, the electrochemical enhancement at a high current density (5 C) mainly originates from the favourable electric conductivity afforded by PEDOT-PSS rather than from Li^+ diffusion characteristics in the bulk. The enhancement of surface kinetics maximized the rate capability for Li^+ insertion into the NE, whereas D_{Li} is more closely related to the bulk reaction of the materials. As previously reported, the improved electric conductivity of the NE can reduce the charge-transfer resistance by lowering the activation energy associated with the Li^+ insertion process at the electrode/electrolyte interface [33–38]. As a result, the incorporated PEDOT-PSS effectively facilitates the charge transfer reactions at the surface of soft carbon through the interface, leading to the superior rate capability of the PE-1.0 NE as compared with the bare NE.

The power characteristics of LICs are generally determined by the NE because Li^+ insertion and extraction involved in the NE is more sluggish than its counter reactions on the surface of the PE. In this regard, it is important to improve the rate capability of the NE in advance in order to build a robust and high-performance LIC. To examine the feasibility of the proposed NE, a LIC full-cell was assembled with activated carbon PE and PP-1.0 NE, as described in Table S2. The PP-1.0 NE was pre-lithiated with 80% of the NE capacity (16.3 mAh) by electrochemical charging to 0.01 V using an auxiliary metallic Li electrode prior to cell operation. After pre-lithiation, the cell was galvanostatically charged and discharged in a voltage range of 1.5–3.9 V at current densities ranging from 0.2 C (17 mA g^{-1}) to 200 C (17 A g^{-1}). For comparison, another LIC full-cell composed of an activated carbon PE and a bare NE was also tested under the same operating conditions.

At a current density of 0.2 C, the LICs employing the bare NE and the PP-1.0 NE delivered similar discharge capacitances of approximately 9.9 F, as shown in Fig. 5a. As the applied current density increased, however, the LIC with the PP-1.0 NE exhibited a higher capacitance up to 100 C. These results are mainly attributed to the improved electrochemical characteristics of the PP-1.0 NE by incorporation of PEDOT-PSS. As suggested, the PEDOT-PSS

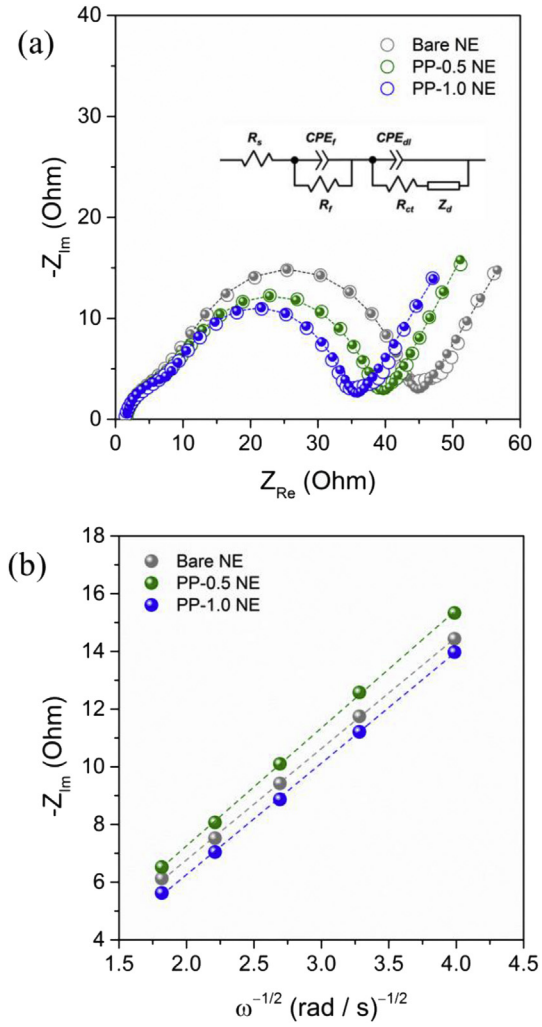

Fig. 4. (a) Nyquist plots of the ac-impedance spectra obtained for all NEs at fully charged state and (b) corresponding Warburg impedance Z_{im} as a function of $\omega^{-1/2}$.

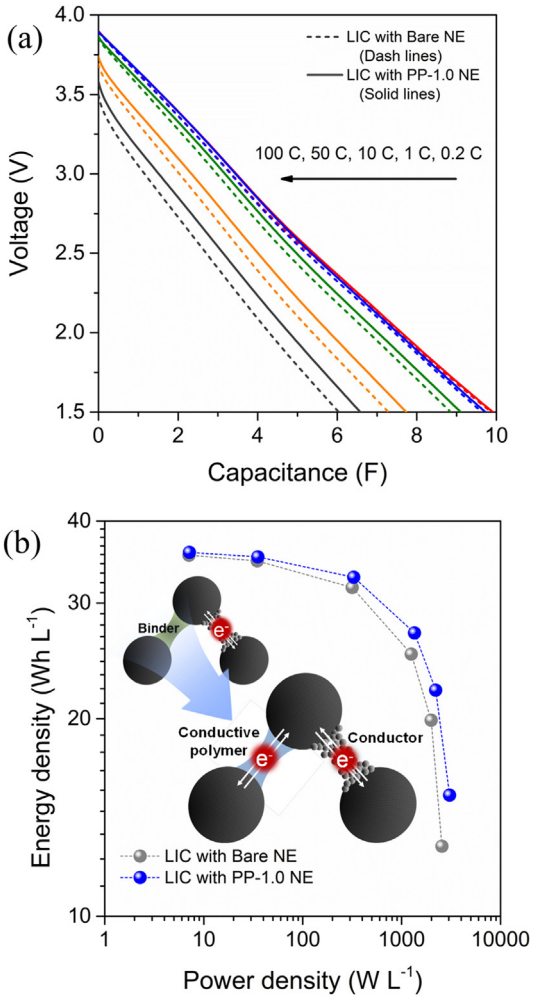

Fig. 5. (a) Rate capabilities of LICs employing the bare and PP-1.0 NEs obtained at various current densities ranging from 0.2 C to 100 C, and corresponding (b) Ragone plots.

Table 2
Electrochemical resistance of the bare, PP-0.5, and PP-1.0 NEs.

Sample	R_s (Ω)	R_f (Ω)	R_{ct} (Ω)
Bare NE	1.5	6.7	35.5
PP-0.5 NE	1.5	6.4	30.9
PP-1.0 NE	1.5	6.4	26.8

incorporated in the NE provides additional electron conduction pathways, which are responsible for facilitating the surface kinetics and reducing the electrical and charge transfer resistance associated with electron−Li^+ reaction in the LIC. As compared with the bare NE, the improved electric conductivity of the PP-1.0 NE afforded by PEDOT-PSS incorporation enabled maximal utilization of the PE in the LIC, with a reduced overpotential during cell operation (Fig. S7). As a result, the LIC employing the PP-1.0 NE had a more reduced IR drop, with a capacitance of 6.6 F (66.7% of the capacitance at 0.2 C) and a 6.1% higher retention than the bare NE (6.0 F, 60.6% of the capacitance at 0.2 C). The enhancement of the power characteristic of the LIC induced by PEDOT-PSS incorporation is also presented in Ragone plots (energy density *vs.* power density) in Fig. 5b. The LIC employing the PP-1.0 NE has a slightly higher energy density than the one with a bare NE for power densities ranging from 100 to 4000 W kg^{-1}. This improvement is attributed to the higher capacitance retention of the LIC employing the PP-1.0 NE as the power density increases.

Fig. 6a shows the cycle performance of LICs employing bare NE and PP-1.0 NE during 5000 cycles at a current density of 10 C (850 mA g^{-1}). From around the 2000th cycle onwards, noticeable capacity fading of the LIC with the bare NE was observed. After 5000 cycles, only 63.3% of the capacitance was retained in the LIC with the bare NE. In contrast, the full-cell with PP-1.0 NE showed more stable cycle performance up to 5000 cycles and the capacitance retention was estimated to be 84.7%. According to previous works by Takamura et al. and Veeraraghavan et al., the better conductivity leads to better utilization of the material in electrodes, resulting in higher capacity retention during repeated cycles [39,40]. The positive effect of PEDOT-PSS incorporation into the NE on the cycle performance is also clearly revealed in the impedance spectra recorded after the 1st, 1000th, and 5000th cycle. After the 1st cycle, similar resistance was found in the LIC with the bare NE and PP-1.0 NE (Fig. 6b). However, the internal resistance of the LIC with the bare NE was clearly greater after the 1000th and 5000th cycles. Since non-Faradaic reactions are mainly involved in the PE, the obtained semi-circles are closely related to the electrochemical behaviour of the respective NEs. Thus, we suggest that a high electric conductivity of PEDOT-PSS induces a reduction of the semi-

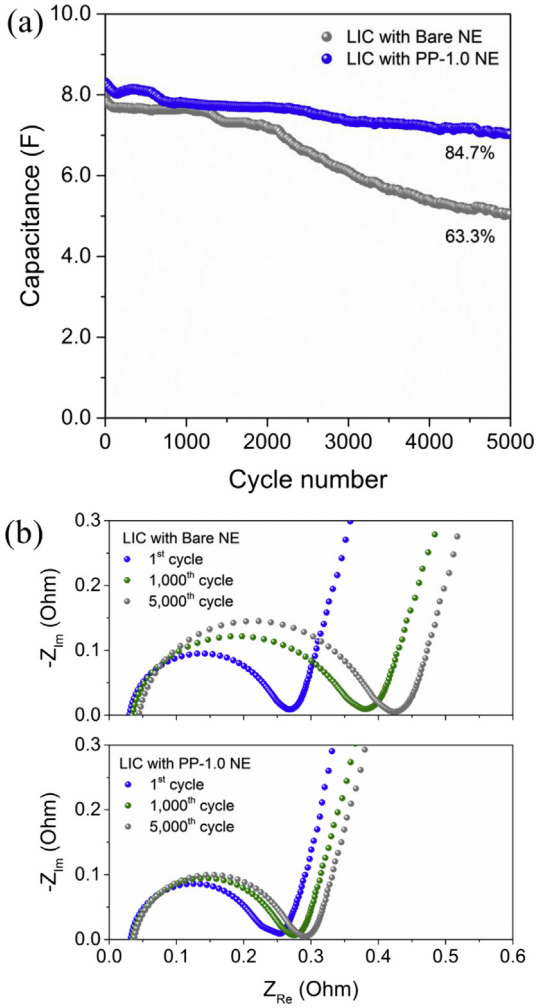

Fig. 6. (a) Capacitance retention of LICs employing bare NE and PP-1.0 NE during 5000 cycles at a constant current density of 10 C in a voltage range from 1.5 to 3.9 V. (b) EIS result obtained from LICs employing bare NE and PP-1.0 NE at selective cycles (after 1st, 1000th, and 5000th cycle).

circle in the EIS results, responsible for lowering charge transfer resistance in the NEs [39,41–43]. This could indeed lead to degraded cycle performance. The favourable electron networks achieved through the addition of PEDOT-PSS to the NE therefore secure enhanced electrochemical performance.

4. Conclusion

PEDOT-PSS, a conductive additive, was added to NEs as a part of the binding material, and its effect on the rate capability of soft carbon electrodes toward Li^+ insertion and extraction was investigated. It was confirmed that the incorporation of PEDOT-PSS was effective for increasing the electrical conductivity of the NE and reducing the charge transfer resistance, thereby providing enhanced rate capability, in particular for Li^+ insertion during charging. This positive effect of PEDOT-PSS addition is also reflected in the electrochemical behaviours of LICs. A noticeable improved power capability of LICs can be attained by reducing the charge transfer resistance and improving the exchange current density. The addition of PEDOT-PSS to NEs thus ensures enhanced energy and power densities of LICs. In conclusion, the addition of appropriate amounts of PEDOT-PSS is beneficial to the electrochemical performance of LICs.

Acknowledgements

This work was supported by the Energy Efficiency & Resources Core Technology Program [20132020102020 and 20132010101890] of the Korea Institute of Energy Technology Evaluation and Planning (KETEP), which granted financial resources from the Ministry of Trade, Industry & Energy (MOTIE), Republic of Korea.

We also acknowledge the finacial support from the R&D Convergence Program (National Resarch Council of Science & Technology, Project No. CAP-14-2-KITECH) of Republic of Korea.

Appendix A. Supplementary data

Supplementary data related to this article can be found at http://dx.doi.org/10.1016/j.jpowsour.2015.08.083.

References

[1] A.K. Shukla, A. Banerjee, M.K. Ravikumar, A. Jalajakshi, Electrochemical capacitors: technical challenges and prognosis for future markets, Electrochim. Acta 84 (2012) 165–173.
[2] L. Wei, M. Sevilla, A.B. Furetes, R. Mokaya, G. Yushin, Polypyrrole-derived activated carbons for high-performance electrical double-layer capacitors with ionic liquid electrolyte, Adv. Funct. Mater. 22 (2012) 827–834.
[3] B.G. Pollet, I. Staffell, J.L. Shang, Current status of hybrid, battery and fuel cell electric vehicles: from electrochemistry to market prospects, Electrochim. Acta 84 (2012) 235–249.
[4] P. Thounthong, V. Chunkag, P. Sethakul, S. Sikkabut, S. Pierfederici, B. Davat, Energy management of fuel cell/solar cell/supercapacitor hybrid power source, J. Power Sources 196 (2011) 313–324.
[5] Y. Qiu, X. Zhang, S. Yang, High performance supercapacitors based on highly conductive nitrogen-doped graphene sheets, Phys. Chem. Chem. Phys. 13 (2011) 12554–12558.
[6] K. Naoi, S. Ishimoto, J. Miyamoto, W. Naoi, Second generation 'nanohybrid supercapacitor': evolution of capacitive energy storage devices, Energy Environ. Soc. 5 (2012) 9363–9373.
[7] W. Gu, G. Yushin, Review of nanostructured carbon materials for electrochemical capacitor applications: advantages and limitations of activated carbon, carbide-derived carbon, zeolite-templated carbon, carbon aerogels, carbon nanotubes, onion-like carbon, and graphene, Wiley Interdiscip. Rev. Energy Environ. 3 (2014) 424–473.
[8] G.G. Amatucci, F. Badway, A. Du Pasquier, T. Zheng, An asymmetric hybrid nonaqueous energy storage cell, J. Electrochem. Soc. 148 (2001) A930–A939.
[9] Z. Fan, J. Yan, T. Wei, L. Zhi, G. Ning, T. Li, F. Wei, Asymmetric supercapacitors based on graphene/MnO_2 and activated carbon nanofiber electrodes with high power and energy density, Adv. Funct. Mater 21 (2011) 2366–2375.
[10] Z. Tang, C.-h. Tang, H. Gong, A high energy density asymmetric supercapacitor from nano-architectured $Ni(OH)_2$/carbon nanotube electrodes, Adv. Funct. Mater. 22 (2012) 1272–1278.
[11] H. Gao, F. Xiao, C.B. Ching, H. Duan, High-performance asymmetric supercapacitor based on graphene hydrogel and nanostructured MnO_2, Appl. Mater. Interfaces 4 (2012) 2801–2810.
[12] N. Omar, M. Daowd, O. Hegazy, M. Al Sakka, Th Coosemans, P. Van den Bossche, J. Van Mierlo, Assessment of lithium-ion capacitor for using in battery electric vehicle and hybrid electric vehicle applications, Electrochim. Acta 86 (2012) 305–315.
[13] M.-S. Park, Y.-G. Lim, S.M. Hwang, J.H. Kim, J.-S. Kim, S.X. Dou, J. Cho, Y.-J. Kim, Scalable integration of Li_5FeO_4 towards robust, high-performance lithium-ion hybrid capacitors, ChemSusChem 7 (2014) 3138–3144.
[14] C. Decaux, G. Lota, E. Raymundo-Pinero, E. Frackowiak, F. Beguin, Electrochemical performance of a hybrid lithium-ion capacitor with a graphite anode preloaded from lithium bis(trifluoromethane)sulfonimide-based electrolyte, Electrochim. Acta 86 (2012) 282–286.
[15] S.R. Sivakkumar, A.G. Pandolfo, Evaluation of lithium-ion capacitors assembled with pre-lithiated graphite anode and activated carbon cathode, Electrochim. Acta 65 (2012) 280–287.
[16] M.-S. Park, Y.-G. Lim, J.-H. Kim, Y.-J. Kim, J. Cho, J.-S. Kim, A novel lithium-doping approach for an advanced lithium ion capacitor, Adv. Energy Mater. 1 (2011) 1002–1006.
[17] H.-G. Jung, M.W. Jang, J. Hassoun, Y.-K. Sun, B. Scrosati, A high-rate long-life $Li_4Ti_5O_{12}$/Li $[Ni_{0.45}Co_{0.1}Mn_{1.45}]O_4$ lithium-ion battery, Nat. Commun. 2 (2011) 516–520.
[18] K. Naoi, W. Naoi, S. Aoyagi, J. Miyamoto, T. Kamino, New generation "nanohybrid supercapacitor", Acc. Chem. Res. 46 (2013) 1075–1083.
[19] Y. Ma, B. Ding, G. Ji, J.Y. Lee, Carbon-encapsulated F-doped $Li_4Ti_5O_{12}$ as a high rate anode material for Li^+ Batteries, ACS Nano 7 (2013) 10870–10878.
[20] M. Schroeder, M. Winter, S. Passerini, A. Balducci, On the use of soft carbon and propylene carbonate-based electrolytes in lithium-ion capacitors, J. Electrochem. Soc. 159 (2012) A1240–A1245.

[21] M. Schroeder, M. Winter, S. Passerini, A. Balducci, On the cycling stability of lithium-ion capacitors containing soft carbon as anodic material, J. Power Sources 238 (2013) 388–394.
[22] G.A. Snook, P. Kao, A.S. Best, Conducting-polymer-based supercapacitor devices and electrodes, J. Power Sources 196 (2011) 1–12.
[23] L.-X. Yuan, Z.-H. Wang, W.-X. Zhang, X.-L. Hu, J.-T. Chen, Y.-H. Huang, J.B. Goodenough, Development and challenges of $LiFePO_4$ cathode material for lithium-ion batteries, Energy Environ. Sci. 4 (2011) 269–284.
[24] J. Han, L. Li, P. Fang, R. Guo, Ultrathin MnO_2 nanorods on conducting polymer nanofibers as a new class of hierarchical nanostructures for high-performance supercapacitors, J. Phys. Chem. C 116 (2012) 15900–15907.
[25] S. Zhou, H. Zhang, Q. Zhao, X. Wang, J. Li, F. Wang, Graphene-wrapped polyaniline nanofibers as electrode materials for organic supercapacitors, Carbon 52 (2013) 440–450.
[26] D.-J. Yun, H. Ra, S.-W. Rhee, Concentration effect of multiwalled carbon nanotube and poly(3, 4-ethylenedioxythiophene) polymerized with poly(4-styrenesulfonate) conjugated film on the catalytic activity for counter electrode in dye sensitized solar cells, Renew. Energy 50 (2013) 692–700.
[27] N.K. Unsworth, I. Hancox, C.A. Dearden, P. Sullivan, M. Walker, R.S. Lilley, J. Sharp, T.S. Jones, Comparison of dimethyl sulfoxide treated highly conductive poly(3,4-ethylenedioxythiophene):poly(styrenesulfonate) electrodes for use in indium tin oxide-free organic electronic photovoltaic devices, Org. Electron 15 (2014) 2624–2631.
[28] J.-S. Yeo, T.-H. Park, M.-H. Seo, J. Miyawaki, I. Mochida, S.-H. Yoon, Solid electrolyte interphase formation behavior on well-defined carbon surfaces for Li-ion battery systems, Electrochim. Acta 77 (2012) 111–120.
[29] J.H. Lee, W.H. Shin, M.-H. Ryou, J.K. Jin, J. Kim, J.W. Choi, Functionalized graphene for high performance lithium ion capacitors, ChemSusChem 5 (2012) 2328–2333.
[30] K.-J. Kim, T.-S. Lee, H.-G. Kim, S.-H. Lim, S.-M. Lee, A hard carbon/microcrystalline graphite/carbon composite with a core-shell structure as novel anode materials for lithium-ion batteries, Electrochim. Acta 135 (2014) 27–34.
[31] C. Ho, I.D. Raistrick, R.A. Huggins, Application of A-C techniques to the study of lithium diffusion in tungsten trioxide thin films, J. Electrochem. Soc. 127 (1980) 343–350.
[32] P. Yu, B.N. Popov, J.A. Ritter, R.E. White, Determination of the lithium ion diffusion coefficient in graphite, J. Electrochem. Soc. 146 (1999) 8–14.
[33] A. Funabiki, M. Inaba, T. Abe, Z. Ogumi, Stage transformation of lithium-graphite intercalation compounds caused by electrochemical lithium intercalation, J. Electrochem. Soc. 146 (1999) 2443–2448.
[34] H. Huang, E.M. Kelder, J. Schooman, Graphite–metal oxide composites as anode for Li-ion batteries, J. Power Sources 97–98 (2001) 114–117.
[35] T. Abe, Y. Mizutami, N. Kawabata, M. Inaba, Z. Ogumi, Effect of co-intercalated organic solvents in graphite on electrochemical Li intercalation, Synth. Met. 125 (2001) 249–253.
[36] T. Abe, H. Fukuda, Y. Iriyama, Z. Ogumi, Solvated Li-ion transfer at interface between graphite and electrolyte, J. Electrochem 151 (2004) A1120–A1123.
[37] K. Xu, "Charge-transfer" process at graphite/electrolyte interface and the solvation sheath structure of Li^+ in nonaqueous electrolytes, J. Electrochem 154 (2007) A162–A167.
[38] M. Mancini, F. Nobili, S. Dsoke, F. D'Amico, R. Tossici, F. Croce, R. Marassi, Lithium intercalation and interfacial kinetics of composite anodes formed by oxidized graphite and copper, J. Power Sources 190 (2009) 141–148.
[39] T. Takamura, M. Saito, A. Shimokawa, C. Nakahara, K. Sekine, M. Maeno, N. Kibayashi, Charge/discharge efficiency improvement by the incorporation of conductive carbons in the carbon anode of Li-ion batteries, J. Power Sources 90 (2000) 45–51.
[40] B. Veeraraghavan, J. Paul, B. Haran, B. Popov, Study of polypyrrole graphite composite as anode material for secondary lithium-ion batteries, J. Power Sources 109 (2002) 377–387.
[41] S.S. Zhang, K. Xu, T.R. Jow, EIS study on the formation of solid electrolyte interface in Li-ion battery, Electrochim. Acta 51 (2006) 1636–1640.
[42] P.L. Moss, G. Au, E.J. Plichta, J.P. Zheng, Investigation of solid electrolyte interfacial layer development during continuous cycling using ac impedance spectra and micro-structural analysis, J. Power Sources 189 (2009) 66–71.
[43] J. Guo, A. Sun, X. Chen, C. Wang, A. Manivannan, Cyclability study of silicon–carbon composite anodes for lithium-ion batteries using electrochemical impedance spectroscopy, Electrochim. Acta 56 (2011) 3981–3987.